ISSN 0016-7029, Geochemistry International, 2007, Vol. 45, No. 10, pp. 983–997. © Pleiades Publishing, Ltd., 2007.
Original Russian Text © Z.M. Voloshina, V.K. Karzhavin, A.V. Bazai, 2007, published in Geokhimiya, 2007, No. 10, pp. 1070–1084.

Metamorphic Evolution of Mineral Assemblages in the Layered Unit and Its Host Rocks of the Eastern Part of the Pana Massif, Kola Peninsula

Z. M. Voloshina, V. K. Karzhavin, and A. V. Bazai

Geological Institute, Kola Research Center, Russian Academy of Sciences, ul. Fersmana 14, Apatity, Murmansk oblast, 184209 Russia

e-mail: voloshina@geoksc.apatity.ru

Received April 10, 2006

Abstract—The paper presents data on the mineral assemblages and chemical composition of minerals in rocks from the eastern part of the Pana Massif, Kola Peninsula, and the results obtained by studying the amphibolization of rocks of this massif genetically related to metamorphism. The rocks contain four amphibole populations, which can be used as good indicators for metamorphic facies. The amphiboles show broad compositional variability. Their evaluated *P–T* crystallization conditions indicate that the prograde stage of the overprinted metamorphic processes occurred at temperatures increasing from 382 to 473°C and pressures from 1.7 to 4.3 kbar. The retrograde stage (biotitization, chloritization, silification, and carbonatization) took place at temperatures of about 370°C and pressures of approximately 1 kbar. The fluid regime of the metamorphic transforms was also controlled by the temperature: the fluids were oxidizing early in the course of the process and gradually became more reducing with decreasing temperature.

DOI: 10.1134/S0016702907100035

INTRODUCTION

The Pana Tundra Massif is part of the single Fedorovo–Pana layered intrusion in the central part of the Kola Peninsula, in the junction zone of the Upper Archean Central Kola block and the Imandra–Varzuga zone of the Karelides, and belongs to the Lower Proterozoic peridotite–pyroxenite–gabbro–norite association [1, 2]. The Pana Massif consists of two discrete blocks: Western Pana (25 km long) and Eastern Pana (55 km), which differ in size, geological structure, rock compositions, and the intensity of metamorphic transforms. Our research was centered mostly on the eastern termination of the Eastern Pana block at the contact of the Belye Tundry alkaline granites in the north and Early Proterozoic volcanic–sedimentary rocks of the Imandra–Varzuga zone in the south.

The Eastern Pana block is dominated by gabbro and leucogabbro, which account for 50–60% of this block by volume and occur mostly in the upper part of the massif. The rest of its vertical section (close to 35 vol %) is made up of gabbronorites, which are concentrated mostly in the lower part of the massif, and various olivine-bearing rocks (approximately 5 vol %) with minor amounts of pyroxenites, norites, anorthosites, and pegmatoid gabbroids [3]. In the pinch-out zone of the Eastern Pana block, the thicknesses of the gabbronorite and gabbro zones drastically decrease. More strongly layered gabbro typically alternates with texturally more monotonous gabbronorite. The relatively thin mineralized unit (MU) contains, along with variably metamorphosed gabbronorite and gabbro, also metanorite, metaanorthosite, and olivine metagabbronorite.

The aim of our research was to characterize the petrology of the rocks and to analyze the evolution of metamorphic processes at the Predgornyi and Kuksha prospects in the pinch-out zone of the Eastern Pana block. For these purposes, we conducted a detailed examination of the petrography of the rocks, a microprobe analysis of their rock-forming and accessory minerals, and determined their crystallization sequence and the *P–T* parameters of these processes. We revealed the character and role of metamorphic processes (including postmagmatic ones) in the formation of the mineral assemblages of the layered unit and barren rocks (BR). It was determined that the development of the metamorphic processes was coupled with systematic variations in the mineralogy of the rocks and the fluid composition in them. The research was conducted on the following samples selected for it: 1–3 from the Predgornyi prospect; 4–7 from the MU in the Kuksha prospect; 9 and 10 from the BR of the massif from their contact with the Imandra–Varzuga complex. The chemical composition of minerals was determined on a Cameca MS-46 X-ray microprobe, and BSE images were taken on a LEO-1450 electron microscope.

Table 1. Microprobe analyses (wt %) of minerals from amphibolized metagabbronorite (sample 1) from the layered unit, Predgornyi prospect

Component	*Pl*	*Opx*	*Cpx*	*Cum*	*Amp*-1	*Amp*-2	*Amp*-3[1]	*Amp*-3	*Bt*	*Ms*
									rim	
SiO_2	47.97	52.24	50.88	56.40	55.58	50.99	42.88	45.49	32.83	48.91
TiO_2	–	0.05	0.13	0.14	0.03	0.43	0.05	0.05	2.29	0.02
Al_2O_3	31.60	0.53	2.31	0.60	2.60	3.71	16.25	14.32	14.71	36.05
FeO	0.20	24.60	8.51	16.92	9.96	15.06	13.00	17.85	16.46	0.98
MnO	–	0.34	0.16	0.53	0.34	0.22	0.19	0.27	0.05	0.00
MgO	–	21.53	13.05	21.68	18.18	13.66	10.44	8.06	11.36	0.69
CaO	16.88	1.02	21.60	0.44	11.70	12.84	13.05	12.66	0.25	0.37
Na_2O	2.70	0.10	2.69	0.06	0.29	0.37	1.60	1.18	0.25	0.59
K_2O	0.03	0.00	0.02	0.05	0.04	0.28	0.38	0.40	7.98	4.43
Cr	–	0.00	0.00	0.00	0.02	0.00	0.00	0.00	0.00	0.00
Ni	–	0.13	0.16	0.14	0.09	0.19	0.06	0.08	1.54	0.00
V	–	0.00	0.00	0.00	0.00	0.05	0.00	0.00	0.71	0.00
Total	99.39	100.54	100.27	96.96	98.83	97.82	97.89	100.34	86.88	92.04
					Cation proportions					
Si	2.22	1.95	1.87	8.02	7.73	7.48	6.28	6.60	2.74	3.18
Al^{IV}	1.73	0.02	0.10	–	0.27	0.52	1.72	1.40	1.44	2.76
Ti	0.00	0.00	0.00	0.02	0.00	0.05	0.01	0.01	0.14	0.00
Al^{IV}	0.00	0.00	0.00	0.10	0.16	0.12	1.09	0.85	0.00	0.00
Fe	0.01	0.77	0.26	2.01	1.16	1.85	1.59	2.17	1.15	0.05
Mn	0.00	0.00	0.01	0.06	0.04	0.03	0.02	0.03	0.00	0.00
Mg	0.00	1.20	0.72	4.60	3.79	2.99	1.28	1.74	1.41	0.07
Ca	0.84	0.04	0.85	0.07	1.75	2.02	2.05	1.97	0.02	0.03
Na	0.24	0.01	0.19	0.02	0.08	0.11	0.05	0.33	0.04	0.08
K	0.00	0.00	0.00	0.01	0.01	0.05	0.10	0.07	0.85	0.43
X_{Fe}	–	39	27	30	23	38	41	55	45	42
An, %	77	–	–	–	–	–	–	–	–	–

Note: Here and in the text, the following mineral symbols and abbreviations are used: *Ab*—albite; *Act*—actinolite; *An*—anorthite; *Ann*—annite; *Bt*—biotite; *Ccp*—chalcopyrite; *Chl*—chlorite; *Cpx*—clinopyroxene; *Czo*—clinozoisite; *Di*—diopside; *En*—enstatite; *Ep*—epidote; *Fac*—ferroactinolite; *Fs*—ferrosilite; *Hbl*—hornblendite; *Hd*—hedenbergite; *Mgt*—magnetite; *Ms*—muscovite; *Opx*—orthopyroxene; *Phl*—phlogopite; *Pl*—plagioclase; *Pn*—pentlandite; *Po*—pyrrhotite; *Py*—pyrite; *Qtz*—quartz; *Ser*—sericite; *Soss*—saussurite; *Ts*—tschermakite; *Vi*—violarite; *Wo*—wollastonite [5]. Subscript numerals near plagioclase symbols (for example, Pl_{An77}) mean the concentration of the anorthite end member, subscript numerals at the symbols of Fe–Mg silicates (for example, Opx_{f39}) mean their total Fe mole fraction, and numerals near amphiboles (for example, *Amp*-1, 2, 3[1], and 3) mean amphibole populations. Dashes correspond to the absence of data. All Fe is recalculated to FeO. The cation proportions of minerals are normalized to 23 oxygens for amphiboles, 11 for biotite and muscovite, 6 for pyroxenes, and 8 for plagioclase.

MINERAL ASSEMBLAGES OF THE LAYERED UNIT AND BARREN ROCKS

The rocks of the Predgorny prospect are characterized by significant metamorphism, which resulted in their amphibolization, biotitization, epidotization, and silification. Some samples contain variably preserved relics of magmatic and autometamorphic minerals.

(1) Amphibolized gabbronorite (Table 1, sample 1) has the following mineral composition: Pl_{An77}–En_{f39}–Di_{f27}–Cum_{f30}–*Amp*-1_{f23}–*Amp*-2_{f38}–*Amp*-3^1_{f41}–*Amp*-3_{f55}–Bt_{f33}–*Ms*–*Czo*–*Ep*–*Qtz*–*Mgt*–*Py*–*Po*–*Ccp*–(*Pn*–*Vi*)[1]. The rock is coarse grained, massive, panidiomorphic granular, amphibolized, and weakly silicified. The primary magmatic minerals are plagioclase, ortho- and clinopyroxene; the secondary minerals are various amphiboles, micas, and minerals of the clinozoisite–epidote series. The ore minerals are magnetite, pyrite, pyrrhotite, chalcopyrite, pentlandite, and violarite.

[1] Mineral symbols and other abbreviations are used according to [4, 5] and listed in the note to Table 1.

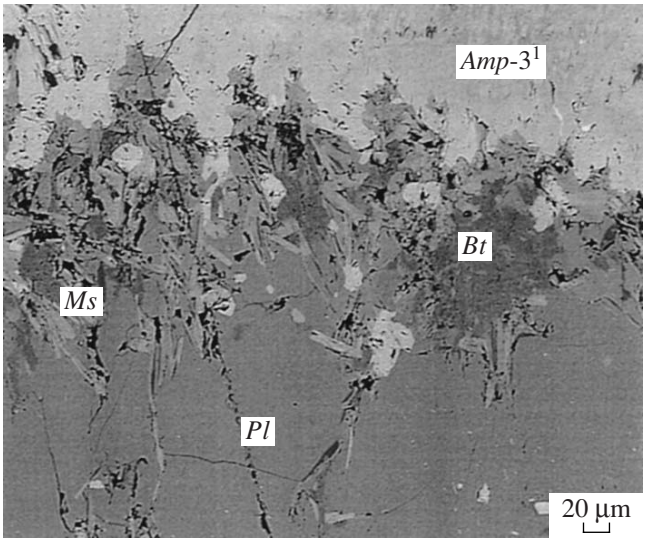

Fig. 1. Fragment of biotite–muscovite (*Bt-Ms*) rim around a plagioclase (*Pl*) grain. Sample 1.

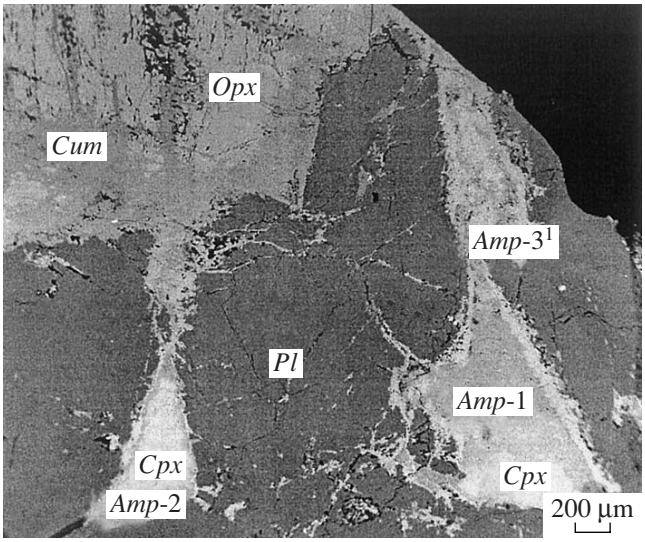

Fig. 2. Plagioclase morphology and general replacement patterns of pyroxene (*Opx* and *Cpx*). Sample 1.

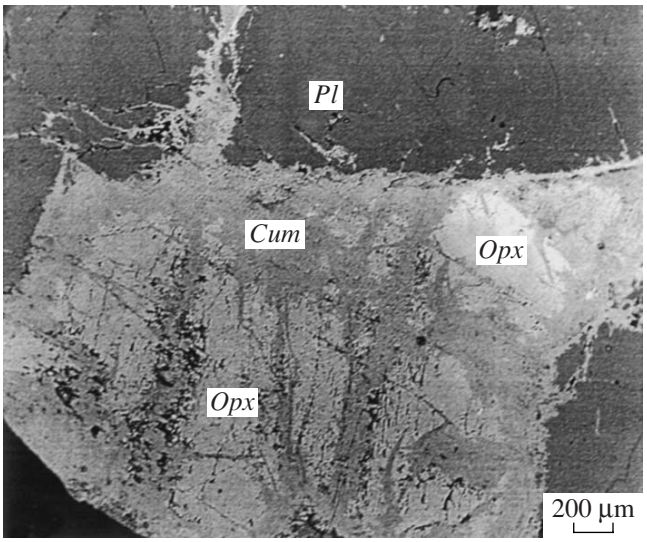

Fig. 3. Orthopyroxene (*Opx*) replacement by cummingtonite (*Cum*). Sample 1.

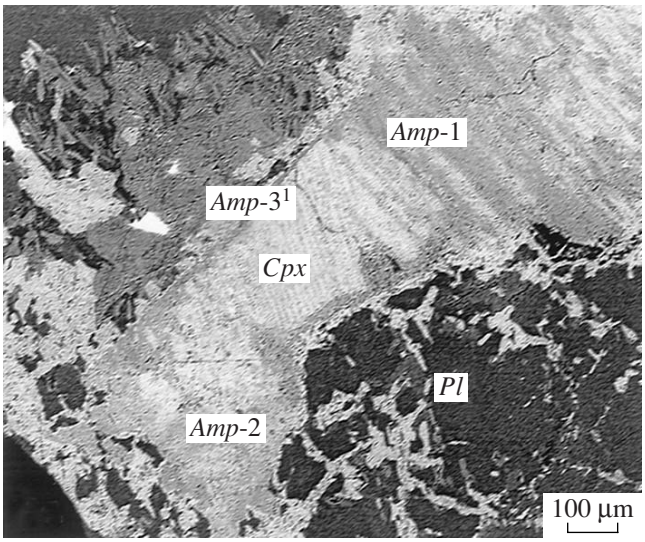

Fig. 4. Relict clinopyroxene grain surrounded by a rim of amphiboles (*Amp*-1, 2, and 3[1]). Sample 1.

The plagioclase is bytownite (Table 1), which forms large, usually rounded unzoned grains. At contacts with amphibole grains, they are surrounded by rims of randomly oriented biotite (predominant) and muscovite flakes (Fig. 1). The pyroxenes are enstatite ($Wo_2En_{60}Fs_{38}$) and diopside ($Wo_{47}En_{40}Fs_{13}$), which are preserved as small relics in amphibole masses (Fig. 2), with orthopyroxene replaced by cummingtonite (*Opx* ← *Cum*; Fig. 3) and clinopyroxene replaced by actinolite and hornblende (*Cpx* ← *Amp*-1 ← *Amp*-2 ← *Amp*-3[1] ← *Amp*-3; Fig. 4). Orthopyroxene is replaced by cummingtonite along cracks and in the peripheries of its grains, up to the development of complete pseudomorphs. The cummingtonite aggregates abound in small interstitial inclusions of ore minerals. The clinopyroxene is also replaced along cracks and in the outermost zones of its grains: first by pale actinolite *Amp*-1 and pale green magnesian hornblende *Amp*-2 and then by bluish green hornblende *Amp*-3[1], which develops in the form of outermost zones in these crystals. Some clinopyroxene grains are replaced by pseudomorphic actinolite *Amp*-1 with rims of green hornblende *Amp*-3 (Fig. 5).

Amphiboles are the most sensitive indicators of mineral-forming and metamorphic conditions in the rocks. According to their chemistry, optical characteris-

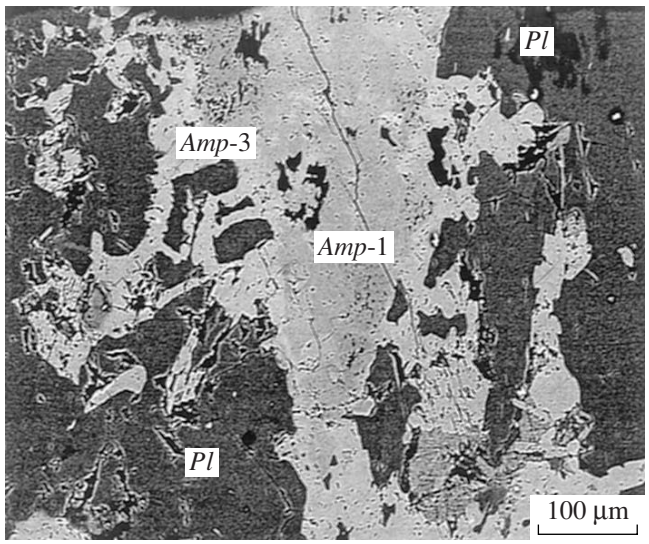

Fig. 5. Zonal amphibole grain: core of early amphibole (*Amp*-1) is surrounded by a rim of younger amphibole (*Amp*-3). Sample 1.

tics, and relations with accompanying minerals, the following four successive amphibole populations were recognized: *Amp*-1–*Amp*-2–*Amp*-3[1]–*Amp*-3. According to the systematics proposed by IMA [5], all of the amphiboles belong to calcic amphiboles: 1—actinolite; 2 and 3—magnesian hornblende; and 3[1]—tschermakite. Recall that all of the aforementioned amphiboles replaced pyroxenes.

The data presented above for the mineral assemblages and compositional variations in certain mineral phases during the growth of their crystals led us to conclude that actinolite *Amp*-1 is the oldest. Magnesian hornblende *Amp*-2 replaced actinolite, and in the course of their growth, its crystals enriched in alumina up to the development of tschermakite rims (*Amp*-3[1]). Magnesian hornblende *Amp*-3 is the youngest and replaced all older calcic amphiboles.

As was mentioned above, biotite and muscovite form rims around plagioclase grains in masses of calcic amphiboles. Moreover, minor biotite amounts may occur among rock-forming minerals as randomly oriented brown flakes. The composition of the mineral corresponds to phlogopite with slightly elevated alumina concentrations.

Minerals of the clinozoisite–epidote series replaced plagioclase in the form of equant and short-columnar grains in saussuritized masses. Quartz composes anhedral grains with weakly undulatory or even extinction in interstices between other minerals.

The ore minerals occur in the interstitial space between grains of rock-forming silicates (Fig. 6) and are mostly associated with early amphiboles and biotite (Fig. 7).

(2) Amphibolized metagabbro have the following mineral composition: Pl_{An74}–*Amp*-1_{f19}–*Amp*-2–*Amp*-3^1–*Amp*-3_{f56}–*Bt*–*Czo*–*Qtz*–*Mgt*–*Py*–*Po*–*Ccp*–*Pn* (Table 2, sample 2); *Pl*-$1_{An\ 68}$–*Pl*-$2_{An\ 60}$–*Pl*-3_{An43}–*Amp*-1_{f17}–*Amp*-2_{f19}–Amp^1_{f43} –*Amp*-3_{f52}–*Bt*–*Czo*–Qtz–*Mgt*–*Py*–*Po*–*Ccp*–*Pn* (Table 2, sample 3). The metagabbro is amphibolized without preservation of any magmatic textures, structures, or minerals and is weakly sheared. The major minerals of the rocks are plagioclase, amphiboles, and clinozoisite; the minor minerals are biotite and quartz; and the ore minerals are magnetite, pyrite, pyrrhotite, chalcopyrite, and violarite.

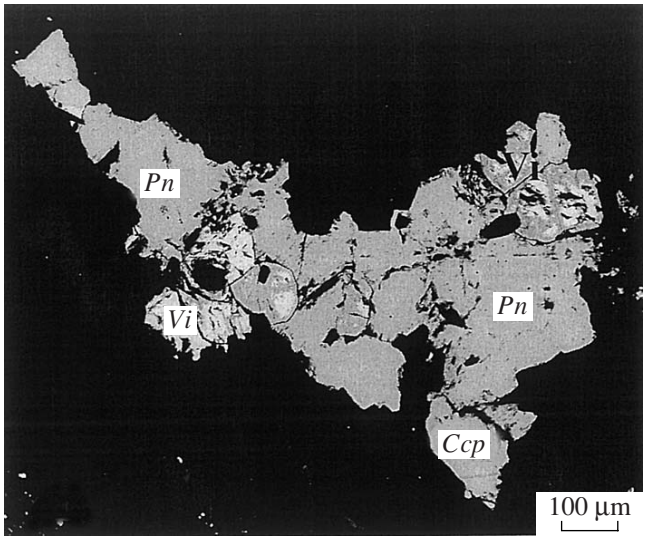

Fig. 6. Morphologies of sulfide grains. Sample 1.

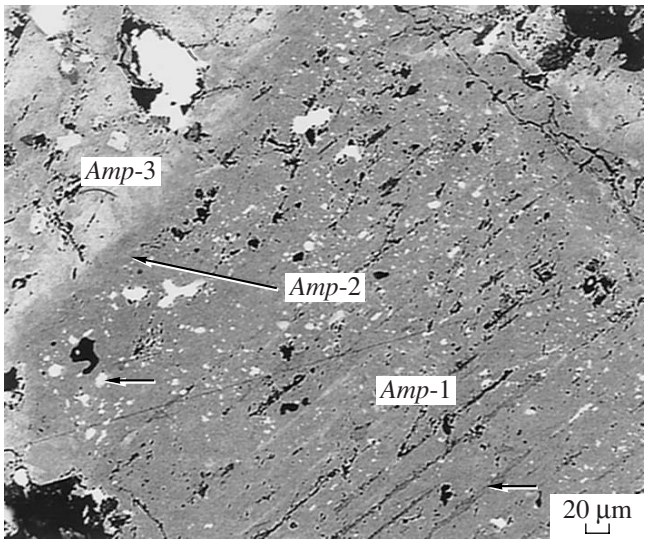

Fig. 7. Zonal amphibole grain (*Amp*-1, -2, -3). Sample 2.

Table 2. Microprobe analyses (wt %) of minerals from amphibolized metagabbronorite (sample 2) and metagabbro (sample 3) from the layered unit, Predgornyi prospect"

Component	Sample 2				Sample 3						
	Pl	*Amp*-1	*Amp*-3[1]	*Amp*-3	*Pl*-1	*Pl*-2	*Pl*-3	*Amp*-1	*Amp*-2	*Amp*-3[1]	*Amp*-3
SiO_2	49.32	56.37	44.21	44.04	50.78	54.63	58.24	56.16	50.06	42.00	44.48
TiO_2	0.00	0.03	0.05	0.23	0.00	0.00	0.00	0.07	0.91	0.24	0.19
Al_2O_3	30.55	2.26	15.40	13.18	29.28	27.38	25.10	1.82	5.04	16.87	11.04
FeO	0.14	7.74	11.88	17.84	0.04	0.09	0.05	7.24	6.77	12.61	16.95
MnO	0.00	0.23	0.26	0.29	0.00	0.00	0.00	0.42	0.33	0.42	0.30
MgO	0.00	18.57	11.16	7.79	0.00	0.00	0.00	19.71	16.04	9.42	8.85
CaO	16.62	14.34	13.46	12.64	14.62	12.46	9.16	12.86	16.27	12.50	11.86
Na_2O	3.15	0.25	1.58	1.22	3.73	4.62	6.68	0.21	0.46	1.31	0.96
K_2O	0.00	0.01	0.08	0.43	0.02	0.02	0.02	0.02	0.02	0.26	0.25
Cr	0.00	0.00	0.00	0.00	0.00	0.00	0.00	0.03	0.04	0.03	0.08
Ni	0.00	0.00	0.03	0.00	0.00	0.00	0.00	0.06	0.04	0.04	0.00
V	0.00	0.00	0.00	0.00	0.00	0.00	0.00	0.02	0.04	0.04	0.07
Total	99.78	99.83	98.11	97.68	98.47	99.20	99.25	98.60	96.02	95.74	95.03
Cation proportions											
Si	2.27	7.77	6.41	6.60	2.35	2.49	2.63	7.80	7.28	6.27	6.80
Al^{IV}	1.66	0.23	1.59	1.40	1.60	1.47	1.34	0.20	0.72	1.73	1.20
Ti	0.00	0.00	0.01	0.00	0.00	0.00	0.00	0.01	0.10	0.03	0.02
Al^{IV}	0.00	0.14	1.04	0.93	0.00	0.00	0.00	0.10	0.14	1.24	0.79
Fe	0.01	0.89	1.44	2.24	0.00	0.00	0.00	0.84	0.02	1.57	2.17
Mn	0.00	0.03	0.03	0.04	0.00	0.00	0.00	0.05	0.04	0.05	0.04
Mg	0.00	3.82	2.41	2.74	0.00	0.00	0.00	4.08	3.47	2.10	2.02
Ca	0.82	2.12	2.09	2.03	0.73	0.61	0.45	1.92	2.53	2.00	1.94
Na	0.28	0.07	0.45	0.36	0.34	0.41	0.59	0.06	0.13	0.38	0.28
K	0.00	0.00	0.01	0.08	0.00	0.00	0.00	0.00	0.00	0.05	0.05
X_{Fe}	–	19	37	56	–	–	–	17	19	43	52
An, %	75	–	–	–	68	60	43	–	–	–	–

The plagioclase of these mineral assemblages occurs as variably shaped grains, some of which are zonal: the anorthite cores are surrounded by rims (a few hundredths of a millimeter thick) of more sodic plagioclase with uneven outlines. We examined a plagioclase grain (Fig. 8, sample 3) consisting of three zones with a gradual decrease in the concentration of the anorthite end member from the core toward margins. The zones were likely formed during the metamorphic recrystallization of the rock: the inner zone consists of bytownite (*An* 68%), the intermediate zone consists of labradorite (*An* 60%), and the outer zone is made up of andesine (*An* 43%). The secondary alterations of the plagioclase involve the formation of minor amounts of sericite, saussurite, and more abundant clinozoisite. Amphiboles were formed in the course of rock alterations (Figs. 2, 4, 8) in the same sequence as in sample 1: *Amp*-1– *Amp*-2–*Amp*-3[1]–*Amp*-3.

(3) The amphibolized leucocratic metagabbro from the Kuksha prospect contain the following mineral assemblages: $Pl\text{-}1_{An72}$–$Pl\text{-}2_{An31}$–$Amp\text{-}1_{f15}$–$Amp\text{-}3_{f17}$–Czo_{f10}–(*Chl*)–*Qtz*–*Mgt*–*Py*–*Po*–*Ccp*–*Pn* (Table 3, sample 4); $Pl\text{-}1_{An60}$–$Pl\text{-}2_{An37}$–$Amp\text{-}1_{f25}$–$Amp\text{-}2_{f28}$–$Amp3_{f44}$–*Czo*–*Bt*–(*Chl*)–*Qtz*–*Mgt*–*Py*–Po–*Ccp*–*Pn* (Table 3, sample 5); $Pl\text{-}1_{An60}$–$Pl\text{-}2_{An22}$–$Amp\text{-}1_{f26}$–$Amp3_{f39}$–*Bt*–$Czof_{10}$–(*Chl*–*Qtz*)–*Mgt*–*Py*–*Po*–*Ccp*–*Pn* (Table 4, sample 6); $Pl\text{-}1_{An62}$–$Pl\text{-}2_{An39}$–$Amp\text{-}1_{f21}$–$Amp\text{-}2_{f27}$–*Czo*–(*Qtz*)–*Mgt*–*Py*– *Po*–*Ccp*–*Pn* (Table 4, sample 7). All metagabbro consist of similar mineral assemblages and have close petrographic characteristics, which suggests that these rocks were produced under similar conditions (Tables 3, 4).

The metagabbroids are medium- to coarse-grained rocks, which are strongly amphibolized and silicified

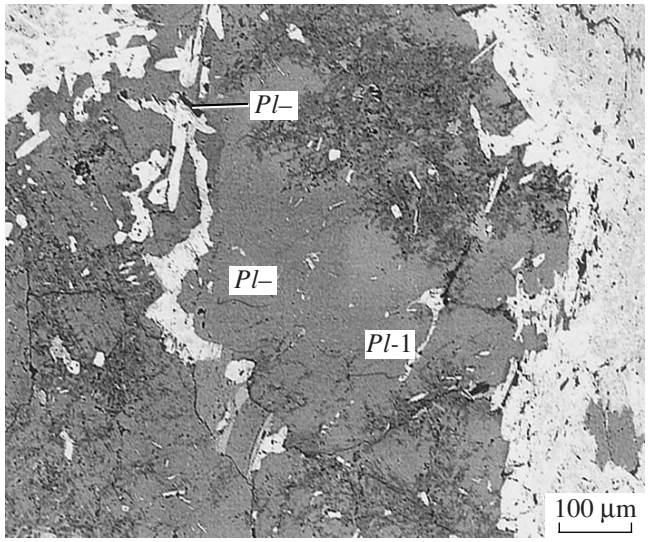

Fig. 8. Zonal plagioclase grain (*Pl*-1—bytownite, *Pl*-2–labradorite, *Pl*-3—andesine). Sample 3.

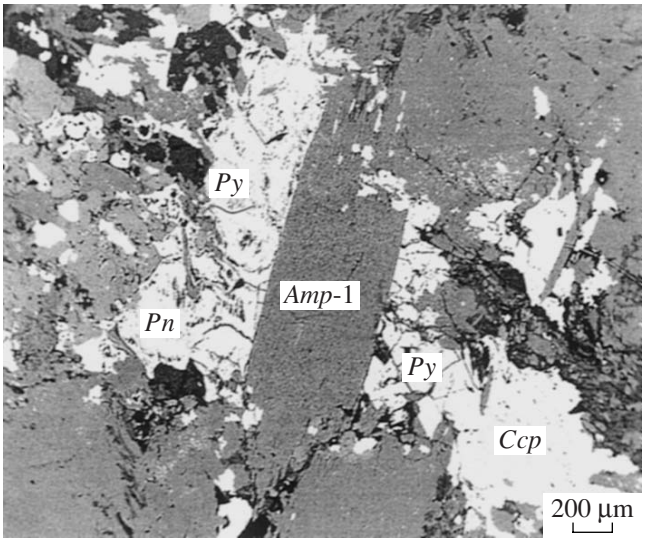

Fig. 9. Early prismatic amphibole-1 cuts across sulfide aggregates. Sample 4.

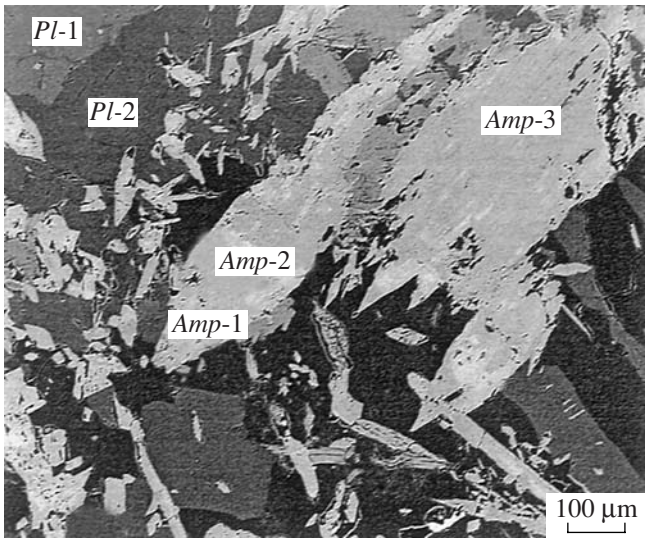

Fig. 10. Zonal amphibole blade-shaped crystals. Sample 5.

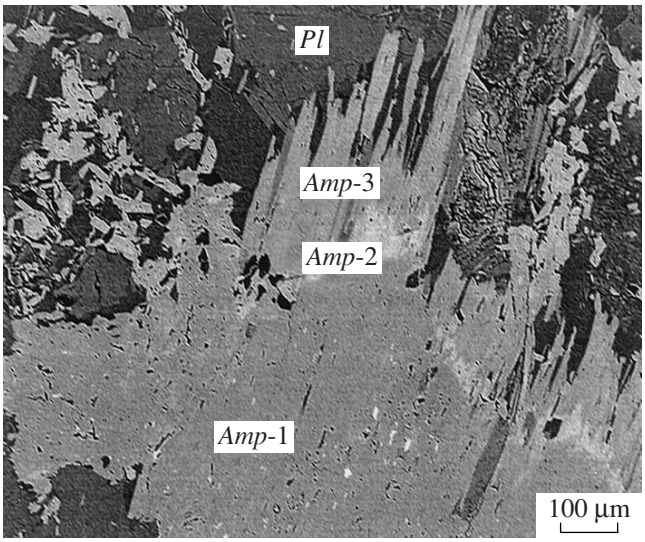

Fig. 11. Platy amphibole blade-shaped crystals. Sample 5.

(sample 5). The rocks are generally characterized by gabbro and hypidiomorphic-granular textures and massive or, sometimes, weakly schistose structures (sample 7). The altered leucocratic metagabbro typically contain no magmatic minerals, and their predominant mineral phases are plagioclase and calcic amphiboles of three populations (*Amp*-3^{I} is absent), along with clinozoisite, quartz, biotite, and chlorite.

As in the rocks described above, plagioclase in this rock group includes grains with normal zoning, i.e., with cores of labradorite–bytownite and peripheral parts of andesine and, more rarely, oligoclase (sample 5). Some plagioclase phenocrysts are strongly saussuritized and contain much clinozoisite.

Similarly to the amphiboles described above, all amphiboles in the metaleucogabbro (Tables 3, 4) are calcic amphiboles. They occur as grains of various shape: prismatic (Fig. 9) or blade-shaped (Fig. 10), with even (Fig. 11) or uneven (Fig. 12) outlines. Amphibole grains are usually zonal and often bear abundant inclusions of ore minerals (Figs. 10–12).

The composition of the amphiboles and their textural relations with neighboring minerals allowed us to distinguish three amphibole populations: *Amp*-1, 2, and 3. As was mentioned above, actinolite *Amp*-1 is the oldest and, as aggregates of randomly oriented prismatic crystals that do not show simultaneous extinction, replaces clinopyroxene with the preservation of the original

Table 3. Microprobe analyses (wt %) of minerals from amphibolized metagabbronorite (samples 4 and 5) from the layered unit, Kuksha prospect

Component	Sample 4					Sample 5				
	Pl-1	*Pl*-2	*Amp*-1	*Amp*-3	*Czo*	*Pl*-1	*Pl*-2	*Amp*-1	*Amp*-2	*Amp*-3
SiO_2	50.51	61.34	56.45	47.11	38.61	52.95	59.50	53.97	52.07	43.67
TiO_2	0.00	0.00	0.00	0.00	0.00	0.00	0.00	0.17	0.20	0.53
Al_2O_3	30.55	23.87	2.25	13.12	27.82	27.87	24.08	3.07	5.23	12.16
FeO	0.21	0.06	6.30	11.34	4.30	0.21	0.06	9.54	10.29	13.41
MnO	0.00	0.00	0.18	0.30	0.08	0.00	0.00	0.27	0.27	0.31
MgO	0.00	0.00	19.55	12.37	0.05	0.00	0.00	16.39	15.13	9.53
CaO	15.41	6.39	14.23	13.45	24.98	13.52	8.06	14.26	14.04	13.57
Na_2O	3.25	7.75	0.21	1.40	0.00	4.84	7.64	0.25	0.52	1.43
K_2O	0.01	0.00	0.01	0.05	0.00	0.07	0.10	0.06	0.16	0.67
Cr	0.00	0.00	0.00	0.00	0.00	0.00	0.00	0.04	0.00	0.00
Ni	0.00	0.00	0.10	0.15	0.00	0.00	0.00	0.03	0.05	0.03
V	0.00	0.00	0.00	0.00	0.00	0.00	0.00	0.02	0.02	0.02
Total	99.94	99.41	99.27	99.29	95.84	99.46	99.44	98.07	97.97	95.33
Cation proportions										
Si	2.31	2.74	7.78	6.71	3.08	2.43	2.68	7.66	7.45	6.62
Al^{IV}	1.65	1.26	0.37	1.29	2.61	1.51	1.28	0.34	0.55	1.38
Ti	0.00	0.00	0.00	0.00	0.00	0.00	0.00	0.02	0.02	0.06
Al^{IV}	–	–	–	0.91	0.00	0.00	0.00	0.17	0.33	0.79
Fe	0.01	0.00	0.73	1.35	0.29	0.01	0.00	1.14	1.23	1.70
Mn	0.00	0.00	0.02	0.04	0.01	0.00	0.00	0.03	0.03	0.04
Mg	0.00	0.00	4.02	2.63	0.01	0.00	0.00	3.47	3.23	2.15
Ca	0.76	0.31	2.10	2.05	2.13	0.66	0.39	2.17	2.15	2.21
Na	0.29	0.67	0.06	0.39	0.00	0.43	0.67	0.07	0.15	0.42
K	0.00	0.00	0.00	0.01	0.00	0.00	0.01	0.01	0.03	0.13
X_{Fe}	–	–	15	34	10	–	–	25	28	44
An, %	72	32	–	–	–	61	36	–	–	–

crystal shapes of this mineral. Smaller elongated grains of *Amp*-1 occur in association with clinozoisite, abound in dust of ore minerals, and are spatially restricted to sulfide segregations. Magnesian hornblende *Amp*-2 replaced actinolite (Figs. 11, 12, 13), and still younger *Amp*-3 composes the outermost zones of crystals of earlier populations. The analysis of amphibole compositions indicates that the successive crystallization in the succession *Amp*-1–*Amp*-2–*Amp*-3 was associated with an increase in the Fe# and, what is the most important, Al# of the amphiboles, with the latter feature likely indicating a systematic temperature increase during the growth of the crystals [6].

Biotite is contained in variable amounts in the rocks. This mineral is the most abundant in the metaleucogabbro from the vicinity of the southern contact of the massif with the host rocks. In this sections, biotite is brown and shows strong pleochroism in yellow-brown shades. The mineral occurs as aggregates in the groundmass of the rocks and can replace amphiboles, a fact suggesting a metamorphic genesis of this mineral.

Table 4. Microprobe analyses (wt %) of minerals from amphibolized metagabbro (samples 6 and 7) from the layered unit, Kuksha prospect

Component	Sample 6						Sample 7				
	Pl-1	*Pl*-2	*Pl*-3	*Amph* 1	*Amph* 3	*Czo*	*Pl*-1	*Pl*-2	*Amph* 1	*Amph* 2	*Czo*
SiO_2	53.17	60.15	63.47	53.95	46.88	38.83	53.43	59.34	55.28	51.11	38.03
TiO_2	0.00	0.00	0.00	0.00	0.27	0.18	0.00	0.00	0.02	0.02	0.02
Al_2O_3	29.03	25.03	22.64	2.59	12.18	28.33	28.61	24.09	2.16	7.78	29.15
FeO	0.09	0.16	0.00	10.93	13.61	5.03	0.04	0.08	8.73	9.80	4.27
MnO	0.00	0.00	0.00	0.27	0.28	0.12	0.00	0.00	0.02	0.04	0.11
MgO	0.00	0.00	0.00	17.34	11.72	0.03	0.00	0.00	18.20	14.50	0.08
CaO	13.51	7.83	5.01	14.14	13.39	26.07	12.82	8.00	13.12	12.36	23.80
Na_2O	4.78	8.33	9.42	0.56	1.03	0.10	4.45	6.99	0.33	0.94	0.11
K_2O	0.17	0.11	0.10	0.19	0.42	0.03	0.02	0.04	0.00	0.05	0.01
Cr	0.00	0.00	0.00	0.00	0.00	0.00	0.00	0.00	0.21	0.01	0.00
Ni	0.00	0.00	0.00	0.00	0.00	0.00	0.00	0.00	0.16	0.06	0.00
V	0.00	0.00	0.00	0.00	0.00	0.00	0.00	0.00	0.02	0.02	0.00
Total	100.74	101.61	100.64	99.97	99.77	98.72	99.36	98.54	98.25	97.12	95.57
Cation proportions											
Si	2.40	2.66	2.80	7.59	6.72	3.03	2.44	2.69	7.72	7.42	3.03
Al^{IV}	1.55	1.30	1.18	0.41	1.28	2.60	1.54	1.29	0.28	0.58	2.74
Ti	0.00	0.00	0.00	0.00	0.03	0.01	0.00	0.00	0.00	0.02	0.00
Al^{IV}	0.00	0.00	0.00	0.02	0.78	0.00	0.00	0.00	0.08	0.73	0.00
Fe	0.00	0.01	0.00	1.29	1.63	0.33	0.00	0.00	1.02	1.17	0.28
Mn	0.00	0.00	0.00	0.03	0.03	0.01	0.00	0.00	0.03	0.04	0.01
Mg	0.00	0.00	0.00	3.64	2.50	0.00	0.00	0.00	3.82	3.10	0.01
Ca	0.65	0.37	0.24	2.13	2.06	2.18	0.63	0.39	1.98	1.90	2.03
Na	0.42	0.71	0.81	0.15	0.29	0.02	0.39	0.61	0.09	0.27	0.02
	0.01	0.01	0.01	0.03	0.08	0.00	0.00	0.00	0.00	0.01	0.00
X_{Fe}	–	–	–	26	39	99	–	–	21	27	10
An, %	60	34	23	–	–	–	62	39	–	–	–

Along with biotite, the rocks also contain chlorite, which preferably developed near contacts with the host rocks (as the biotite did) and rapidly disappears from the rocks away from the contact. Chlorite usually replaces biotite, but sometimes its single flakes occur in the fine-grained actinolite mass. In thin sections, the chlorite is pale green and shows weak pleochroism and low birefringence. As usual, chlorite was produced by the latest retrograde alterations of the rocks (Fig. 12).

Quartz occurs as aggregates of equant grains that fill interstices between larger grains of plagioclase and magnesian hornblende and composes younger monomineralic veinlets.

Sulfides (chalcopyrite, pyrrhotite, pyrite, pentlandite, and violarite) occur as anhedral grains in the interstitial space of rock-forming minerals and as dust disseminated in cleavage planes of amphiboles and clino-

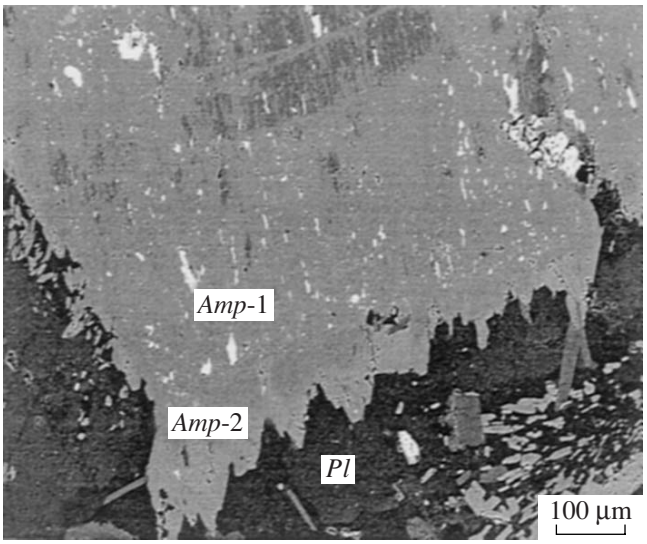

Fig. 12. Jagged margins of zonal amphibole grains. The cores of the amphibole grains contain oriented chains of sulfide grains. Sample 7.

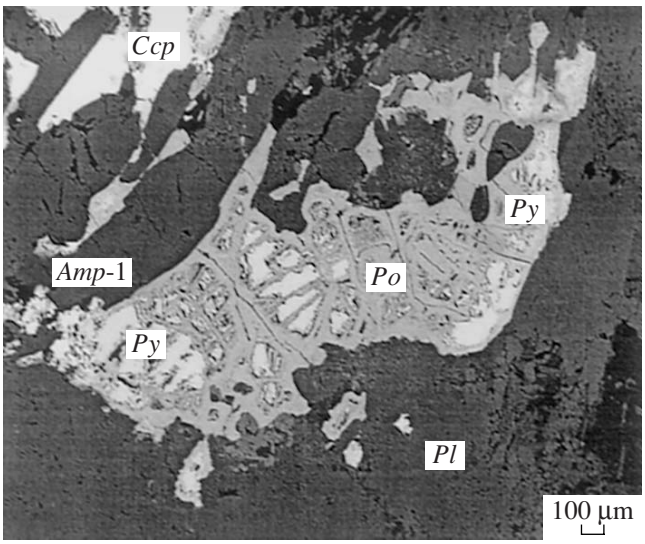

Fig. 13. Morphology of sulfide aggregates. Sample 6.

zoisite (Figs. 13, 14). The leucogabbro contain minor amounts of euhedral apatite prisms.

Mineral Assemblages of Contact Rocks

Within 2 m from their contact with alkaline granites, the medium-grained gabbronorites of the Fedorovo–Pana Massif are cataclased and transformed into tremolite, actinolite, or hornblende schists; are brecciated; and abound in quartz–feldspathic veinlets and veins. Away from the contact, the alkaline granites themselves are pale pinkish gray inequigranular massive porphyritic rocks with locally and weakly pronounced lineation [7].

Mesocratic amphibolized and silicified gabbro-amphibolites with minor amounts of carbonates (Table 5, samples 8, 9) occur near the contact with the metavolcanic rocks of the Imandra–Varzuga zone. The medium-grained gabbro-amphibolite (sample 8) has the following mineralogical composition: Pl_{An34}–*Amp*-1_{f32}–*Amp*-3_{f52}–*Czo*–*Ep*–*Bt*–*Qtz*. The coarse-grained sheared gabbro-amphibolite (sample 9) consists of Pl_{An24}–*Amp*-1_{f35}–*Amp*-3_{f56}–*Czo*–*Ep*–*Bt*–*Cal*–*Qtz*. The plagioclase occurs as anhedral unzoned grains partly replaced by clinozoisite and saussurite. The newly formed hornblende forms large elongated and tabular subhedral grains. The latter often show patchy coloration in thin sections, as is typical of amphiboles in metavolcanic rocks of the Imandra–Varzuga zone. The pale patches have a composition corresponding to *Amp*-1, and the dark green parts correspond to magnesian hornblende *Amp*-3. Some of the crystals abound in minute inclusions of minerals of the plagioclase–clinozoisite groundmass. Biotite is unevenly distributed in the rock: its highest concentrations are contained in rocks closer to the contact with the volcanics. The mineral forms aggregates in the groundmass of the rock, replaces amphibole, and usually occurs in close association with chlorite. In thin sections, biotite is brown, with strong pleochroism in yellow-brown tints.

Thermodynamics and P– T Metamorphic Conditions

The rocks composing the eastern termination of the Pana Massif are characterized by strong metamorphic transforms, first of all, amphibolization. Some samples (for example, sample 1 from the Predgornyi prospect) contain relics of primary magmatic and postmagmatic minerals. Orthopyroxene replacement by cummingto-

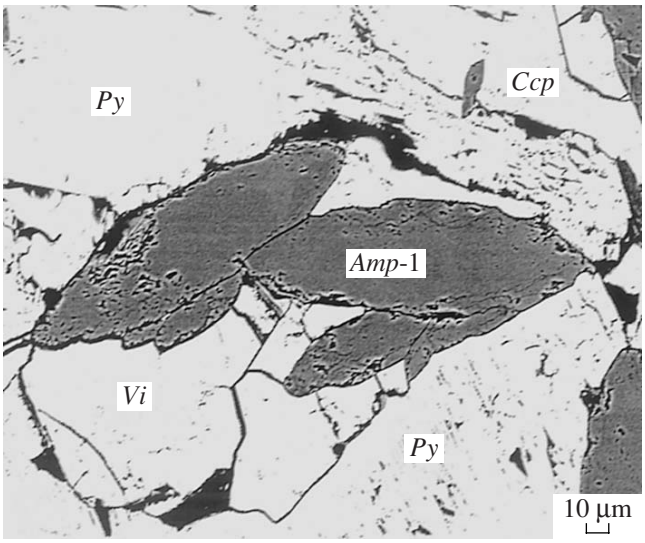

Fig. 14. Morphology of sulfide aggregates. Sample 7.

Table 5. Microprobe analyses (wt %) of minerals from amphibolized gabbroamphibolite (samples 8 and 9) from the barren unit, southern contact zone with the host rocks

Component	Sample 8			Sample 9		
	Pl	*Amp*-1	*Amp*-3	*Pl*	*Amp*-1	*Amp*-3
SiO_2	59.90	54.16	44.80	61.33	52.05	42.68
TiO_2	0.00	0.03	0.20	0.00	0.02	0.28
Al_2O_3	25.21	1.71	11.88	23.38	2.70	13.71
FeO	0.05	13.24	16.84	0.08	13.35	17.22
MnO	0.00	0.23	0.26	0.00	0.32	0.30
MgO	0.00	15.11	8.74	0.00	13.69	7.58
CaO	6.57	13.39	12.36	5.04	12.74	11.35
Na_2O	4.49	0.15	1.25	8.55	0.28	1.37
K_2O	0.01	0.06	0.33	0.02	0.03	0.24
Cr	0.00	0.07	0.00	0.00	0.18	0.05
Ni	0.00	0.00	0.00	0.00	0.00	0.00
V	0.00	0.00	0.00	0.00	0.10	0.07
Total	89.78	98.15	96.66	98.40	95.46	94.86
Cation proportions						
Si	2.68	7.80	6.74	2.76	7.72	6.56
Al^{VI}	1.33	0.20	1.26	1.24	0.28	1.44
Ti	0.00	0.00	0.02	0.00	0.00	0.03
Al^{VI}	0.00	0.09	0.85	0.00	0.19	1.04
Fe	0.00	1.59	2.12	0.00	1.66	2.21
Mn	0.00	0.03	0.03	0.00	0.04	0.04
Mg	0.00	3.24	1.96	0.00	3.03	1.74
Ca	0.32	2.07	1.99	0.24	2.03	1.87
Na	0.65	0.04	0.37	0.75	0.08	0.41
K	0.00	0.01	0.06	0.00	0.01	0.05
X_{Fe}	–	33	52	–	35	56
An, %	33	–	–	24	–	–

nite was related to the processes of autometamorphic replacement of high-temperature minerals by lower temperature phases in the cooling rocks under the effect of decreasing temperature and pressure. The processes of autometamorphic transforms themselves are regarded as the evolution of the magmatic rock [8].

The later metamorphic history of the rocks is recorded in a number of amphibole populations: actinolite, tschermakite, and magnesian hornblende.

According to the results obtained by the plagioclase–amphibole geothermometer [9], the amphiboles of the actinolite–hornblende series crystallized at 450–500°C for amphiboles 1 and 2 and at 600–650°C for amphibole 3. These temperatures seem to be slight overestimates, and hence, during the following stage of our research, we utilized the TWQ method [10] with an internally consistent database appended with thermodynamic values for some amphiboles from [11]. The calculations were conducted with the compositions of minerals from the rocks regardless of the presence of their solid solutions: all clinopyroxenes were assumed to be diopside, all hornblendes were regarded as the magnesian end member of the series, etc.

The intersections of the equilibrium lines for respective chemical reactions in the *P–T* diagram (Fig. 15) cover broad ranges of conditions, from early autometamorphic transforms of the rocks with pyroxene–cummingtonite assemblages (*Opx–Cum*, T = 624°C, P = 6.2 kbar) to the metamorphic transforms of rocks with the early plagioclase–actinolite (*Pl–Act*, T = 382°C, P = 1.7 kbar and *Pl–Act–Ts* T = 398°C, P = 2.6 kbar) and later plagioclase–hornblende assemblages (*Pl–Hbl*, T = 473°C, P = 4.3 kbar) and further to diaphthoritic rocks (*Pl–Act–Chl*, T = 370°C, P = 1 kbar). The chemical reactions and equilibrium constants are as follows:

Pl–Cum assemblage:

1. $9An + 3Cum + 3Di + 2Mgt = 12En + 3Fs + 6Czo + 3O_2$
2. $6Cum + 2Mgt = 3Fs + 21En + 3O_2 + 6H_2O$
3. $Cum + 2Czo = 3An + 3En + Di + 2H_2O$
4. $18An + 6Di + 2Mgt + 6H_2O = 3En + 3Fs + 12Czo + O_2$
5. $Cum + 14Czo + 6Qtz = 21An + 7Di + 8H_2O$

Pl–Act assemblage

1. $Fac + 2Qtz + 6Czo = 5Hd + 9An + 4H_2O$
2. $4An + 16Di + 10Mgt + 36Qtz + 10H_2O = 6Fac + 4Hbl + 5O_2$
3. $12Czo + 72Di + 186Qtz + 50Mgt + 42H_2O = 30Fac + 18Hbl + 25O_2$
4. $30Czo + 12Di + 87Qtz + 20Mgt = 12Fac + 42An + 3Hbl + 10O_2$
5. $24Czo + 10Mag + 48Qtz = 36An + 6Fac + 5O_2 + 6H_2O$
6. $10Mag + 48Qtz + 24Czo = 36An + 6Fac + 5O_2 + 6H_2O$

Pl–Act–Ts assemblage

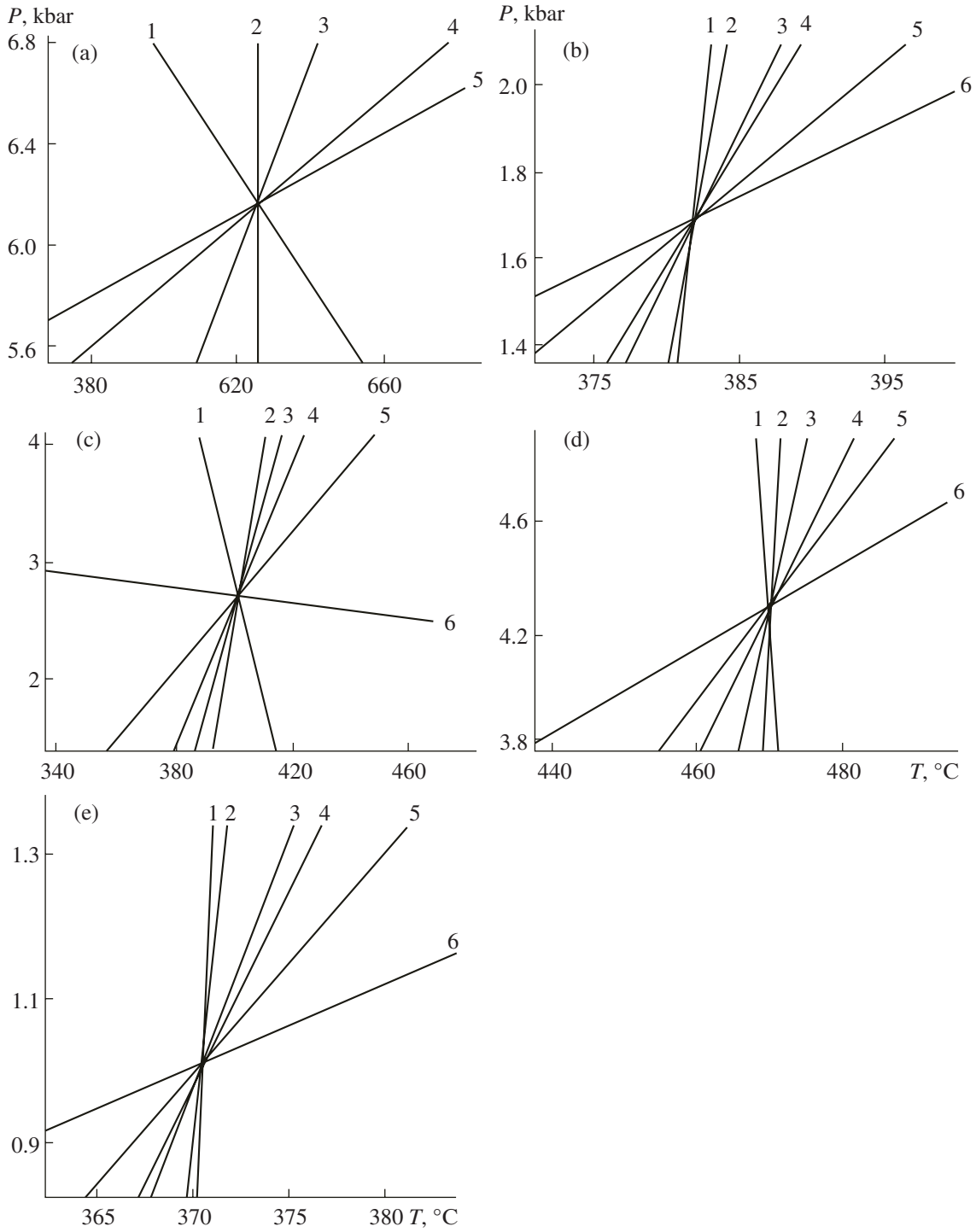

Fig. 15. Evaluation of the *P–T* parameters of equilibrium silicate systems: (a) *Pl–Cum* assemblage; (b) *Pl–Act* assemblage; (c) *Pl–Act–Ts* assemblage; (d) *Pl–Hbl* assemblage; (e) *Pl–Act–Chl* assemblage.

1. $4An + 2Phl + 2Mgt + 4Qtz + 2H_2O = 2Ts + 2Ann + O_2$

2. $12Czo + 9Phl + 42Qtz + 14Mgt + 6H_2O = 3Fac + 9Ts + 9Ann + 7O_2$

3. $12Czo + 24Qtz + 5Mgt = 18An + 3Fac + 4O_2 + 3H_2O$

4. $24Czo + 10Mgt + 48Qtz = 36An + 6Fac + 5O_2 + 6H_2O$

5. $5Ts + Ann + 12Czo + 14Qtz = 3Fac + 28An + 5Phl + 8H_2O$

6. $6Fac + 84An + 24Phl + 14Mag + 30H_2O = 24Ts +$

$24Czo + 24Ann + 7O_2$

Pl–Hbl assemblage

1. $2An + 8Di + 6Qtz + 2Mgt + 2H_2O = 2Hbl + 6Hd + O_2$

2. $Czo + 42Qtz + 24Phl + 14Mag + 6Fac + 6H_2O = 24Ann + 18Hbl + 7O_2$

3. $6Czo + 12Di + 4Mag + 15Qtz = 6An + 3Hbl + 12Hd + 2O_2$

4. $14Mgt + 84An + 30\,Fac + 30H_2O = 64Ann + 48Hd + 24Czo + 7O_2$

5. $6Czo + Hbl + 3Qtz = 10An + 4Di + 4H_2O$

6. $22An + 16Di + 2Mgt + 10H_2O = 4Hbl + 16Hd + 12Czo + O_2$

Pl–Act–Chl assemblage

1. $2An + 10Di + 10Mg + 30Qtz + 14H_2O = 6Fac + 2Chl + 5O_2$

2. $24Czo + 180Di + 588Qtz + 190Mg + 246H_2O = 114Fac + 36Chl + 95O_2$

3. $84Czo + 15Di + 213Qtz + 50Mgt = 123An + 30Fac + 3Chl + 25O_2$

4. $24Czo + 10Mgt + 48Qtz = 36An + 6Fac + 5O_2 + 6H_2O$

5. $12Czo + Chl + 9Qtz = 19An + 5Di + 10H_2O$

6. $196An + 80Di + 30Mgt + 142H_2O = 18Fac + 120Czo + 15O_2$.

The *P–T* estimates presented above for the amphiboles with regard for petrographic data on their crystallization sequence led us to conclude that the *P–T* parameters of the metamorphic transforms define a prograde path from 382 to 473°C and from 1.7 to 4.3 kbar.

Hence, the eastern termination of the Pana Massif was affected by regional metamorphism of the epidote-amphibolite facies, which was overprinted on earlier autometamorphic (at the Predgornyi prospect) and low-temperature greenschist-facies (Predgornyi and Kuksha prospects) transformations of the rocks. Rocks in tectonic zones, at tectonic contacts of the massif with rocks of the Imandra–Varzuga structure, and in the pinch-out zone of the massif show traces of retrograde rock transforms (chloritization and silification) that occurred at lower temperatures and pressures (T = 370°C and P = 1 kbar, chlorite–actinolite subfacies of the greenschist facies).

The regional metamorphism of the supracrustal rocks of the Imandra–Varzuga Complex south of the massif corresponds to the biotite–actinolite subfacies of the greenschist facies. The metamorphic grade northeast of the massif reaches the epidote-amphibolite and amphibolite facies [12]. The data presented above testify to the isofacies character of the mineral assemblages of the rocks composing the massif and those of the host sedimentary–volcanic complex, which led us to the conclusion about the overprinting of Svecofennian regional metamorphism on the rocks of the massif [7].

Physicochemical Simulations

The calculation of the equilibrium composition of phases in a heterogeneous multisystem imitating the process of metamorphism was conducted by a program complex making use of free energy minimization [13]. The physicochemical simulation of multisystems makes it possible to assay the behavior and composition of the fluid phase in equilibrium with silicate and sulfide phases and involves the recalculation of chemical analyses into mole concentrations of elements in 1 kg of the rock. The initial model multisystem for our rock samples from the Eastern Pana block of the massif contained 18 independent components (elements): Al–C–Ca–Cu–Fe–K–Mg–Na–Ni–Pd–Pt–S–Se–Si–Te–Ti–H–O. The calculation matrix of the multisystem was composed of 34 dependent components of silicate–sulfide phases and a fluid phase consisting of ten gaseous components: H_2O, H_2, O_2, CO, CO_2, H_2S, SO_2, S_2, CH_4, and C_2H_6. The identification of major persistent relations in the distributions of fluid components can provide valuable information for solving petrogenetic problems related to the genesis of ore mineralization. These simulations enable the researcher to reproduce the physicochemical situation for the multisystems and to estimate the behavior of components during various stages of the natural process with the evaluation of the composition of the volatile components and the fluid regime as a whole. During this phase, it is possible to evaluate the conditions under which certain mineral assemblages were produced, the compositions of the solid phase, fluid, and correspondingly, the behavior of sulfur and oxygen. The numerical simulation of the model multisystems was carried out by the TWQ techniques for the calculated *P–T* parameters. Table 6 lists the calculated compositions of the solid phases and fluid.

The calculated data presented in the table indicate that the physicochemical conditions varied in the process of metamorphism at the active participation of fluids, which affected the solid phase, including the composition of the mineral assemblages. The variations of the *P–T* parameters during the crystallization of minerals were associated with variations in the composition and concentration of the fluid. The predominant fluid component was water. Its highest activity was determined to occur during autometamorphism and at the epidote-amphibolite facies. The concentrations of other fluid components varied according to variations in the thermodynamic parameters of the natural process and the oxygen partial pressure, which controlled the fluid regime and speciation of C, H, S, and other elements in the natural system. The behavior of H_2O in the natural process was correlated with the activities and concentrations of CO_2, H_2, and CH_4. During the autometamorphic processes at the epidote-amphibolite facies and the

Table 6. Calculated component composition (wt %) of solid phases and fluid in various facies zones

Minerals and fluid components	t = 624°C P = 6.2 kbar	t = 382°C P = 1.7 kbar	t = 398°C P = 2.6 kbar	t = 473°C P = 4.3 kbar	t = 370°C P = 1.0 kbar
	Pl–Cum	*Pl–Act*	*Pl–Act–Ts*	*Pl–Hbl*	*Pl–Act–Chl*
Ab	11.64	11.53	11.49	11.47	19.60
An	39.83	39.44	24.24	18.57	27.50
En	10.85	–	–	–	–
Di	8.67	6.90	–	–	–
Cum	21.60	–	–	–	–
Act	–	31.00	34.27	3.99	32.16
Ts	–	–	22.10	–	–
Hbl	–	–	–	55.77	–
Ann	2.37	0.24	2.35	2.64	–
Phl	–	1.73	–	–	–
Chl	–	–	–	–	6.23
Qtz	1.78	0.85	–	0.31	3.25
Mag	tr	6.68	0.44	tr	5.80
Py	0.24	0.22	0.06	0.34	4.16
Po	–	tr	–	–	–
Ccp	tr	0.78	0.77	–	–
			Gas: partial pressure P_i/fugacity f_i		
H_2	8.8×10^{1}	5.6×10^{1}	1.5×10^{-2}	9.2×10^{-3}	6.6×10^{-2}
	3.1×10^{0}	9.3×10^{1}	3.3×10^{-2}	5.2×10^{-2}	5.1×10^{-2}
H_2O	6.1×10^{3}	1.6×10^{3}	2.6×10^{3}	6.9×10^{3}	1.0×10^{3}
	4.1×10^{3}	2.9×10^{2}	5.0×10^{2}	3.2×10^{2}	5.2×10^{2}
H_2S	1.8×10^{1}	2.1×10^{-1}	6.4×10^{-1}	9.3×10^{-1}	1.1×10^{0}
	1.2×10^{2}	2.2×10^{-1}	1.0×10^{0}	1.1×10^{1}	9.4×10^{-1}
O_2	2.6×10^{-18}	1.2×10^{-33}	1.7×10^{-25}	1.1×10^{-21}	9.5×10^{-28}
	1.5×10^{-17}	2.1×10^{-33}	4.2×10^{-25}	1.2×10^{-20}	1.3×10^{-27}
SO_2	2.1×10^{-2}	1.5×10^{-15}	6.7×10^{-4}	1.4×10^{-1}	1.4×10^{-5}
	2.5×10^{-1}	1.5×10^{-15}	1.2×10^{-3}	3.6×10^{0}	1.0×10^{-5}
CO	3.2×10^{-3}	2.6×10^{-8}	2.3×10^{-5}	3.6×10^{-5}	2.0×10^{-4}
	3.0×10^{-2}	5.4×10^{-8}	7.6×10^{-5}	7.4×10^{-4}	3.1×10^{-5}
CO_2	1.2×10^{1}	1.8×10^{-6}	6.5×10^{0}	1.9×10^{1}	2.8×10^{0}
	9.5×10^{1}	2.4×10^{-6}	1.4×10^{1}	3.0×10^{2}	2.9×10^{0}
CH_4	1.7×10^{-5}	3.6×10^{0}	3.1×10^{-8}	9.3×10^{-10}	3.2×10^{-6}
	1.8×10^{-4}	7.4×10^{0}	1.1×10^{-7}	2.1×10^{-8}	4.6×10^{-6}
C_2H_6	2.4×10^{-14}	6.1×10^{-7}	2.1×10^{-19}	8.8×10^{-22}	3.1×10^{-16}
	6.8×10^{-13}	1.2×10^{-6}	2.9×10^{-19}	7.3×10^{-20}	3.9×10^{-16}
S_2	1.9×10^{-3}	3.2×10^{-15}	8.5×10^{-7}	1.7×10^{-4}	4.1×10^{-8}
	9.0×10^{-2}	4.7×10^{-15}	1.7×10^{-6}	1.3×10^{-3}	5.0×10^{-7}
ΣV_{tot}, cm^3	356.76	356.71	350.19	344.45	410.22
V_{gas}, cm^3	25.17	25.08	19.90	15.91	74.66
Predominant fluid	$H_2O \gg H_2 \geq H_2S \approx CO_2$	$H_2O \gg H_2 > CH_4$	$H_2O \gg H_2 > H_2S$	$H_2O \gg H_2 > H_2S$	$H_2O \gg H_2 \approx H_2S$

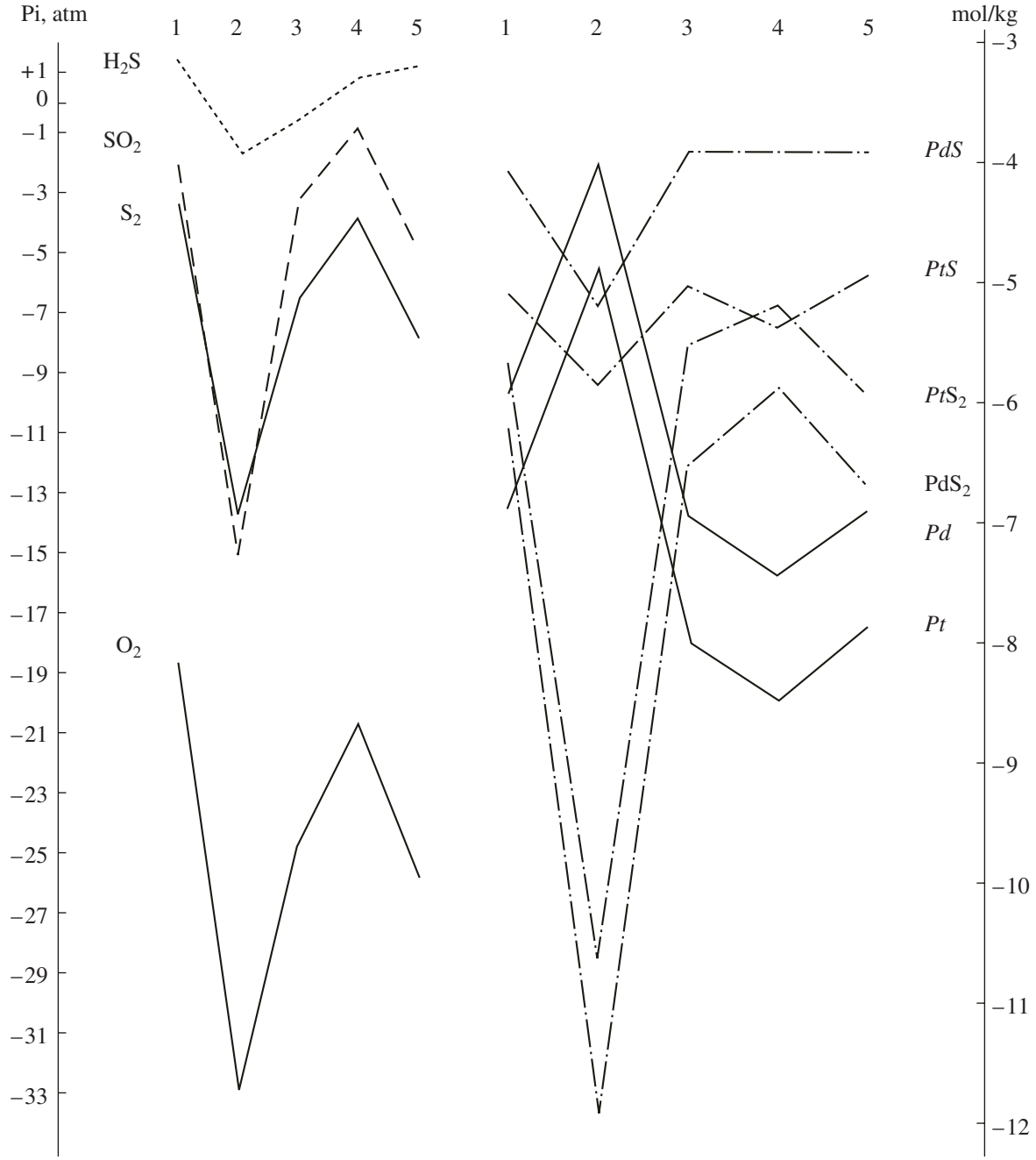

Fig. 16. Behavior of fluid components during metamorphism. (1–5) Mineral assemblages: (1) *Pl–Cum*; (2) *Pl–Act*; (3) *Pl–Act–Ts*; (4) *Pl–Hbl*; (5) *Pl–Act–Chl.*

chlorite–actinolite subfacies, the concentrations of these components in the fluid phase were relatively high.

The transition from the early to late metamorphic stages was associated with certain systematic variations in the concentrations of volatile components related to the evolution from oxidizing to reducing conditions. Note that S-bearing components and S in the fluid are mutually dependent at their relatively high activities. The calculation results indicate that, depending on the *P–T* parameters, sulfur speciation in the system systematically varies and is correlated with variations in the oxygen partial pressure. These variations control the behavior of S-bearing components of the fluid and PGE. The concentration of elemental modes of PGE drastically increase at the greenschist facies (Fig. 16). The two-stage transformations of S-bearing compounds likely involved an inversion in the S valence in S-bearing components with variations in the redox conditions within a certain range of metamorphic tempera-

tures. This phenomenon is consistent with the stable forms and transformations of the solid sulfides [14]. The behavior of fluid components suggests that greenschist-facies conditions serve as a redox barrier for the redistribution of components in the C–H–S–O system. This barrier is likely responsible for the transition from oxidizing (autometamorphism) to reducing conditions with subsequent changes in the temperature and pressure.

CONCLUSIONS

(1) The results of our research indicate that the rocks composing the eastern termination of the Pana intrusion were variably affected by metasomatic transforms, including early autometamorphism, overprinted metamorphism, which was related to the regional metamorphism of the host rocks, retrograde alterations (chloritization, sericitization, and silification), which occurred at lower temperatures and locally, within tectonized zones, and at contacts with the host volcanic–sedimentary complex in the pinch-out zone of the intrusion.

(2) The mineral assemblages contain several populations of amphiboles, which are sensitive indicators of metamorphic facies and can be utilized to obtain thermobarometric estimates. The mineral assemblages correspond to the specifics conditions of metamorphism.

(3) The metamorphic processes were determined to have been associated with variations in the concentrations of some gaseous components (H_2, CO_2, CH_4, H_2S, and others). The fluid regime thereby varied from oxidizing during the high-temperature metamorphism ($Po_2 \approx 10^{-16}$) to reducing during low-temperature regional metamorphism ($Po_2 \approx 10^{-35}$ to 10^{-25}) and at the overprinting of later metamorphic stages ($Po_2 \approx 10^{-22}$ to 10^{-20}).

ACKNOWLEDGMENTS

The authors thank S.A. Karpov for consultations and provided materials.

REFERENCES

1. V. S. Dokuchaeva, "Petrology and Ore Formation Conditions in the Fedorova–Pana Intrusion" in *Geology and Genesis of the PGE Deposits* (Nauka, Moscow, 1994), pp. 65–79 [in Russian].
2. *Precambrian Magmatic Formations of the Northeastern Baltic Shield*, Ed. by I. V. Bel'kova (Nauka, Leningrad, 1985) [in Russian].
3. Z. M. Voloshina, V. P. Petrov, A. E. Borisov, et al., "Metamorphic Mineral Assemblages in Rocks Composing the Eastern Pana Block of the Pana Tundra Intrusions," Zap. Vseross. Mineral. O-va, No. 1, 16–26 (2000).
4. Kretz. R. "Symbols for Rock-Forming Minerals," Am. Mineral. **68**, 277–279 (1983).
5. "Amphibole Nomenclature: Report of Subcommission on Amphiboles, Commission on New Minerals and Mineral Names of the International Mineralogical Association (CNMMN IMA)," Zap. Vseross. Mineral. O-va, No. 6, 82–102 (1997).
6. D. A. Velikoslavinskii, *Comparative Characteristics of the Moderate- and Low-Pressure Regional Metamorphism* (Nauka, Moscow, 1973) [in Russian].
7. Z. M. Voloshina, V. P. Petrov, V. K. Karzhavin, et al., "Mineral Formation and *P–T* Parameters in the Pana Layered Intrusion, Kola Peninsula, at the Contact with Country Rocks," Geokhimiya, No. 4, 365–374 (2002) [Geochem. Int. **40**, 323–331 (2002)].
8. G. M. Saranchina and N. F. Shinkarev, *Petrology of Magmatic and Metamorphic Rocks* (Nedra, Leningrad, 1973) [in Russian].
9. L. L. Perchuk, *Equilibrium of Rock-Forming Minerals* (Nauka, Moscow, 1970) [in Russian].
10. R. G. Berman, "Thermobarometry Using Multiequilibrium Calculation: A New Technique with Petrological Applications," Can. Mineral. **29**, 833–855 (1991).
11. V. K. Karzhavin, "Amphiboles. Thermodynamic Properties," Geokhimiya, No. 12, 1724–1732 (1991).
12. *Imandra–Varzuga Zone of the Karelides*, Ed. by G. I. Gorbunova (Nauka, Leningrad, 1982) [in Russian].
13. I. K. Karpov, A. I. Kiselev, and F. A. Letnikov, *Computer Simulation of the Natural Mineral-Forming Processes* (Nedra, Moscow, 1976) [in Russian].
14. V. K. Karzhavin and Z. M. Voloshina, "Simulation of Metamorphism and Fluid Regime in the Mineralized Unit of the Pana Massif in Relation to Its PGE Ore Mineralization," Geokhimiya, No. 5, 522–531 (2006) [Geochem. Int. **44**, 475–484 (2006)].